Journal of Alloys and Compounds 728 (2017) 241–252

Contents lists available at ScienceDirect

Journal of Alloys and Compounds

journal homepage: http://www.elsevier.com/locate/jalcom

Novel ternary semiconductor $CdLa_2X_4$ (X=S or Se) single crystal with efficient second harmonic generation in the visible spectral range

A.H. Reshak

New Technologies - Research Centre, University of West Bohemia, Univerzitni 8, 306 14, Pilsen, Czech Republic

A R T I C L E I N F O

Article history:
Received 7 June 2017
Received in revised form
3 August 2017
Accepted 23 August 2017
Available online 1 September 2017

Keywords:
Second harmonic generation
Ternary semiconductor
Non-centro-symmetric
$CdLa_2X_4$ (X=S or Se)
DFT

A B S T R A C T

Comprehensive *ab-inito* calculations are performed to investigate the suitability of the non-centro-symmetric $CdLa_2S_4$ and $CdLa_2Se_4$ for using as nonlinear optical crystals in visible spectral range. The calculations reveal the direct band gap nature of both compounds with large absorption coefficient (10^4 cm^{-1}). The absorption edges of $CdLa_2S_4$ and $CdLa_2Se_4$ occur at $\lambda = 579.3$ nm and $\lambda = 670.1$ nm, and the optical band gaps are estimated to be 2.14 eV and 1.85 eV for $CdLa_2S_4$ and $CdLa_2Se_4$, respectively. $CdLa_2S_4$ exhibits SHG of about two times of the well-known KH_2PO_4 (KDP) single crystals which exhibits a nonlinear coefficient of 0.39 p.m./V. Whereas $CdLa_2Se_4$ exhibits SHG very close to the experimental value of that for the well-known $KTiOPO_4$ (KTP) which exhibits a nonlinear coefficient of about 14.6 ± 1.0.

1. Introduction

In recent years, tremendous research work have been done for the development of different varieties of novel inorganic and organic nonlinear optical materials (NLO) [1]. The NLO materials exhibit promising applications for second harmonic generation (SHG), sum or difference frequency mixing, optical parametric oscillation (OPO) or amplification (OPA) and as efficient photonic devices [2–8]. The SHG is an NLO phenomenon which is related to the nonlinear electrical susceptibility. Developing highly efficient NLO crystals for visible, ultra-violet (UV) and deep-UV applications is important for laser spectroscopy and laser processing, including laser-tailoring of molecules and optical triggering [9–13].

The ternary semiconductor compounds AB_mC_n (A = Cu, Ag, Zn, Cd, ….; B= Al, Ga, In, La, … and C=S, Se, Te with chalcopyrite structure have attracted considerable attention in recent years due to their applications in optical sensing, light-emitting diodes, biological labeling, solar cells, magnetic and as photocatalysts [14–24]. The non-centro-symmetric ternary semiconductor chalcogenide, $CdLa_2S_4$ and $CdLa_2Se_4$ have a strong absorption in the visible light region and, therefore, they become good nonlinear optical (NLO) crystals which can produce efficient second harmonic generation (SHG) in the visible light region. Tremendous research work has been done on the photocatalytic performance of these materials [14–24]. However, to date, no comprehensive work neither experimental data or first principles calculations on the structural, electronic, linear and nonlinear optical properties of $CdLa_2X_4$ (X = S or Se) have appeared in the literature. Therefore, as a natural extension to previous existing works, the detailed depiction of the electronic structure, linear and nonlinear optical properties of $CdLa_2X_4$ (X = S or Se) using full potential method is timely and would bring us important insights in understanding the origin of the linear and nonlinear optical properties. Hence, it is very important to use a full potential method based on the density functional theory (DFT). The full-potential method [25] within different types of exchange correlation (XC) potentials, namely general gradient approximation (PBE-GGA) [26] and the modified Becke-Johnson potential (mBJ) [27], are used to ascertain the influence of the XC on the resulting band gap, and hence, on the linear and nonlinear optical properties of $CdLa_2X_4$ (X = S or Se). In this work, *ab-inito* calculations are performed to investigate the linear and nonlinear optical properties of the non-centro-symmetric $CdLa_2X_4$ (X = S or Se) for using as efficient NLO materials in the visible spectral region.

2. Methodology aspect

Two ternary semiconductor compounds with non-centro-symmetric chalcopyrite structure are used to investigate their

E-mail address: maalidph@yahoo.co.uk.

http://dx.doi.org/10.1016/j.jallcom.2017.08.235
0925-8388/

linear and nonlinear optical properties. These are $CdLa_2S_4$ and $CdLa_2Se_4$ with tetragonal symmetry ($I\bar{4}2d$) and lattice parameters $\mathbf{a} = \mathbf{b} = 8.5919900$ Å, $\mathbf{c} = 9.00872271$ Å and Z = 4 for $CdLa_2S_4$ [28], and $\mathbf{a} = \mathbf{b} = 8.93262736$ Å, $\mathbf{c} = 9.40390262$ Å and Z = 4 for $CdLa_2Se_4$ [29]. The crystal structure of $CdLa_2S_4$ and $CdLa_2Se_4$ are formed through a combination of the covalent CdX_4 and LaX_4 structural units (Fig. 1). The x-ray structural data [28,29] are used as input to calculate the electronic band structure and, hence, the linear and nonlinear optical properties of $CdLa_2S_4$ and $CdLa_2Se_4$. The geometrical structures are optimized using the full-potential method (wien2k package [25]) within the generalized gradient approximation (PBE-GGA) [26]. The resulting relaxed geometrical structures are used to calculate the ground state properties utilizing the recently modified Becke-Johnson potential (mBJ) [27]. To reach accurate results, the muffin-tin spheres (R_{MT}) are chosen in such a way that the spheres did not overlap. Therefore, to insure that no charge leakage is left out of the atomic sphere cores, the $R_{MT's}$ are chosen to be 2.5 atomic unit (a.u.) for Cd, La, and Se while it is 2.31 a.u. for S. We should emphasize that, to achieve the total energy convergence, the basis functions in the interstitial region (IR) are expanded up to $R_{MT} \times K_{max} = 7.0$ and inside the atomic spheres for the wave function, the $\boldsymbol{l}_{max}$ is taken to be equal 10, and the charge density is Fourier expanded up to$G_{max} = 12(a.u.)^{-1}$. A mesh of 1000 $\vec{k}$ points in the irreducible Brillouin zone (IBZ) is used to obtained the self-consistency which is converged since the total energy of the system is stable within 0.00001 Ry. The ground state properties, and hence the linear and nonlinear optical properties are obtained using 50000 $\vec{k}$ points in the IBZ. The input required for linear and nonlinear optical properties calculation are the energy eigenvalues and eigenfunctions which are the natural outputs of the band structure calculation.

In recent years, due to the improvement of the computational technologies, it has been proven that the first-principles calculation is a strong and useful tool to predict the crystal structure and properties related to the electron configuration of a material before its synthesis [30–38]. It is well know that the DFT approaches have the ability to accurately predict the ground state properties of the materials, and the developed analysis tools are vital to investigating their intrinsic mechanism. This microscopic understanding has further guided molecular engineering design for new crystals with novel structures and properties. It is anticipated that first-principle material approaches highly improve the search efficiency and greatly help scientists to save resources in the exploration of new materials with good performance [30–38].

We would like to mention that, in our previous works [39–43], we have calculated the linear and nonlinear optical properties and the energy band gaps using full potential method for several systems whose linear and nonlinear optical properties and energy band gaps are known experimentally and a very good agreement with the experimental data was obtained. Thus, we believe that our calculations reported in this paper would produce very accurate and reliable results which will greatly help to develop the experiments and save resources in the exploration of new NLO crystals with appropriate linear and nonlinear optical performance. The present study is aimed at the NLO properties of the non-centrosymmetric $CdLa_2S_4$ and $CdLa_2Se_4$ crystals.

The linear optical properties are calculated using the optical code implemented in the wien2k package [25], for more details see the user guide [44] and ref. 45. The nonlinear optical properties are calculated using the NLO code, which is compatible with the Wien2k package, see refs. 46,47. $CdLa_2S_4$ and $CdLa_2Se_4$ crystallizes in the non-centro-symmetric with tetragonal symmetry ($I\bar{4}2d$). This symmetry allows three non-zero components of the second-order dielectric (optical) tensor corresponding to the electric field $\vec{E}$ being directed along $\mathbf{a}$, $\mathbf{b}$, and $\mathbf{c}$-crystallographic axes. We identify these with the x,y and z Cartesian directions.

These are $\varepsilon^{xx}(\omega) = \varepsilon^{yy}(\omega) = \varepsilon^{\perp}(\omega)$and $\varepsilon^{zz}(\omega) = \varepsilon^{\perp}(\omega)$. The imaginary part of the principal complex tensor components completely defines the linear optical susceptibilities. The imaginary part of the principal complex tensor components originates from inter-band transitions between valence and conduction band states. According to the dipole selection rule, only transitions changing the angular momentum quantum number l by unity are allowed. The imaginary parts of the optical function's dispersion were calculated using the following expression which is taken from Ref. 44:

$$\varepsilon_2^{ij}(\omega) = \frac{8\pi^2\hbar^2e^2}{m^2V}\sum_k\sum_{cv}(f_c - f_v)\frac{p_{cv}^i(k)p_{vc}^j(k)}{E_{vc}^2}\delta[E_c(k) - E_v(k) - \hbar\omega] \tag{1}$$

where m, e and $\hbar$are the electron mass, charge and Planck's constant, respectively. f_c and f_v represent the Fermi distributions of the conduction and valence bands, respectively. The term $p_{cv}^i(k)$ denotes the momentum matrix element transition from the energy level c of the conduction band to the level v of the valence band at certain $\mathbf{k}$-point in the BZ and V is the unit cell volume.

The complex second-order nonlinear optical susceptibility tensor $\chi_{ijk}^{(2)}(-2\omega;\omega;\omega)$ can be generally written as [46–49]:

$$\chi_{\text{inter}}^{ijk}(-2\omega;\omega,\omega) = \frac{e^3}{\hbar^2}\sum_{nml}\int\frac{d\vec{k}}{4\pi^3}\frac{\vec{r}^{\,i}_{nm}\left\{\vec{r}^{\,j}_{ml}\vec{r}^{\,k}_{ln}\right\}}{(\omega_{ln} - \omega_{ml})}\left\{\frac{2f_{nm}}{(\omega_{mn} - 2\omega)} + \frac{f_{ml}}{(\omega_{ml} - \omega)} + \frac{f_{ln}}{(\omega_{ln} - \omega)}\right\} \tag{2}$$

$$\chi_{\text{intra}}^{ijk}(-2\omega;\omega,\omega) = \frac{e^3}{\hbar^2}\int\frac{d\vec{k}}{4\pi^3}\left[\sum_{nml}\omega_{nm}\vec{r}^{\,i}_{nm}\left\{\vec{r}^{\,j}_{ml}\vec{r}^{\,k}_{ln}\right\}\left\{\frac{f_{nl}}{\omega_{ln}^2(\omega_{ln} - \omega)} - \frac{f_{lm}}{\omega_{ml}^2(\omega_{ml} - \omega)}\right\} - 8i\sum_{nm}\frac{f_{nm}\vec{r}^{\,i}_{nm}\left\{\Delta^j_{mn}\vec{r}^{\,k}_{nm}\right\}}{\omega_{mn}^2(\omega_{mn} - 2\omega)} + 2\sum_{nml}\frac{f_{nm}\vec{r}^{\,i}_{nm}\left\{\vec{r}^{\,j}_{ml}\vec{r}^{\,k}_{ln}\right\}(\omega_{ml} - \omega_{ln})}{\omega_{mn}^2(\omega_{mn} - 2\omega)}\right]. \tag{3}$$

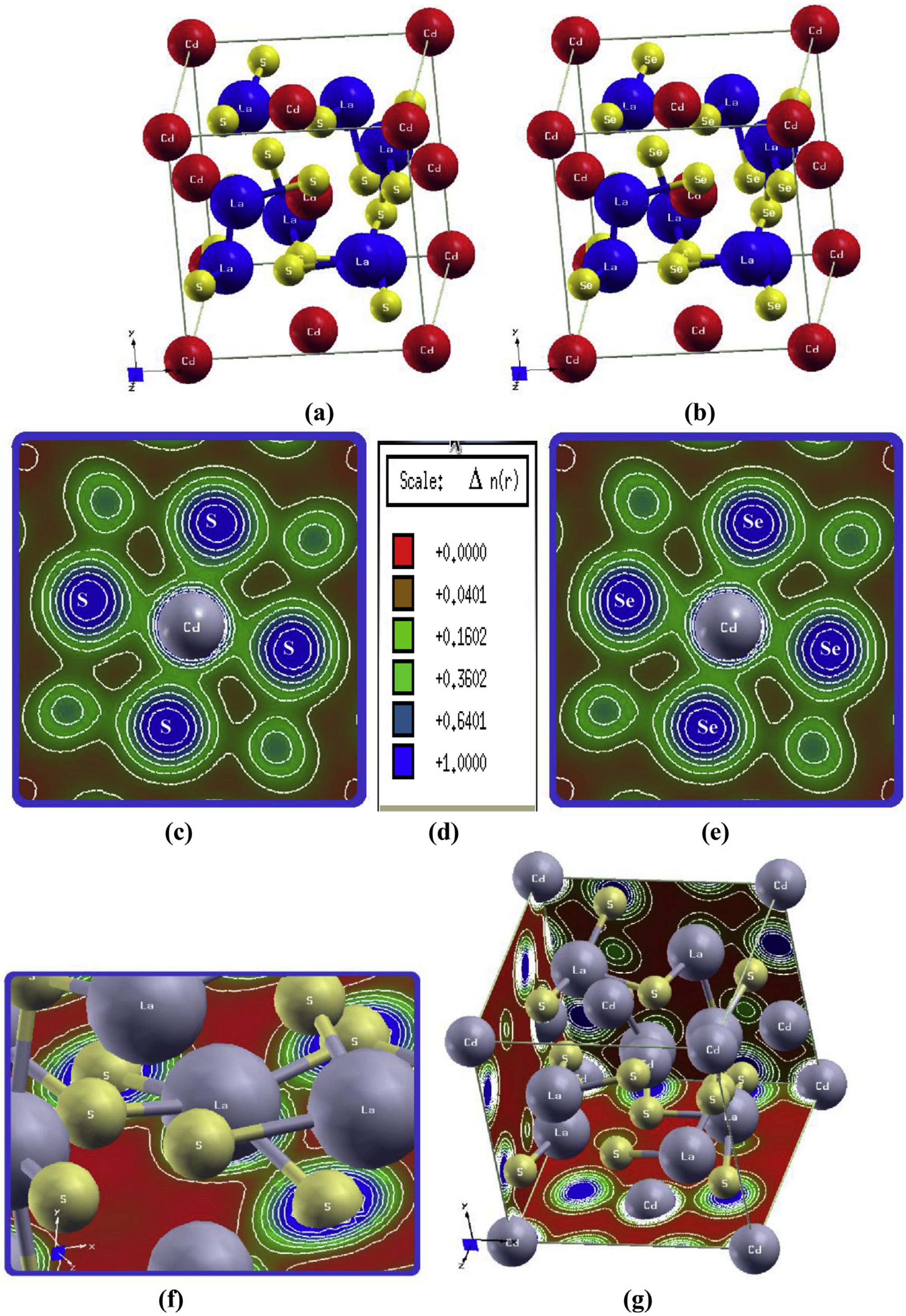

Fig. 1. (**a**–**b**) Crystal structure of $CdLa_2S_4$ and $CdLa_2Se_4$ with tetragonal symmetry ($I\bar{4}2d$) and lattice parameters **a** = **b** = 8.5919900 Å, c = 9.00872271 Å and Z = 4 for $CdLa_2S_4$, and **a** = **b** = 8.93262736 Å, c = 9.40390262 Å and Z = 4 for $CdLa_2Se_4$. The crystal structure of $CdLa_2S_4$ and $CdLa_2Se_4$ forms through a combination of the covalent CdX_4 and LaX_4 structural units; (**c**–**g**) The charge density distribution of $CdLa_2S_4$ and $CdLa_2Se_4$ which shows an efficient charge transfer occurs towards Cd, S or Se atoms, as the Cd, S or Se atoms are surrounded by uniform spheres of charge density and the maximum charge accumulates around Cd, S or Se atoms as indicated by the blue color, the thermoscale show the blue color indicates the maximum charge intensity (1.0000). (For interpretation of the references to colour in this figure legend, the reader is referred to the web version of this article.)

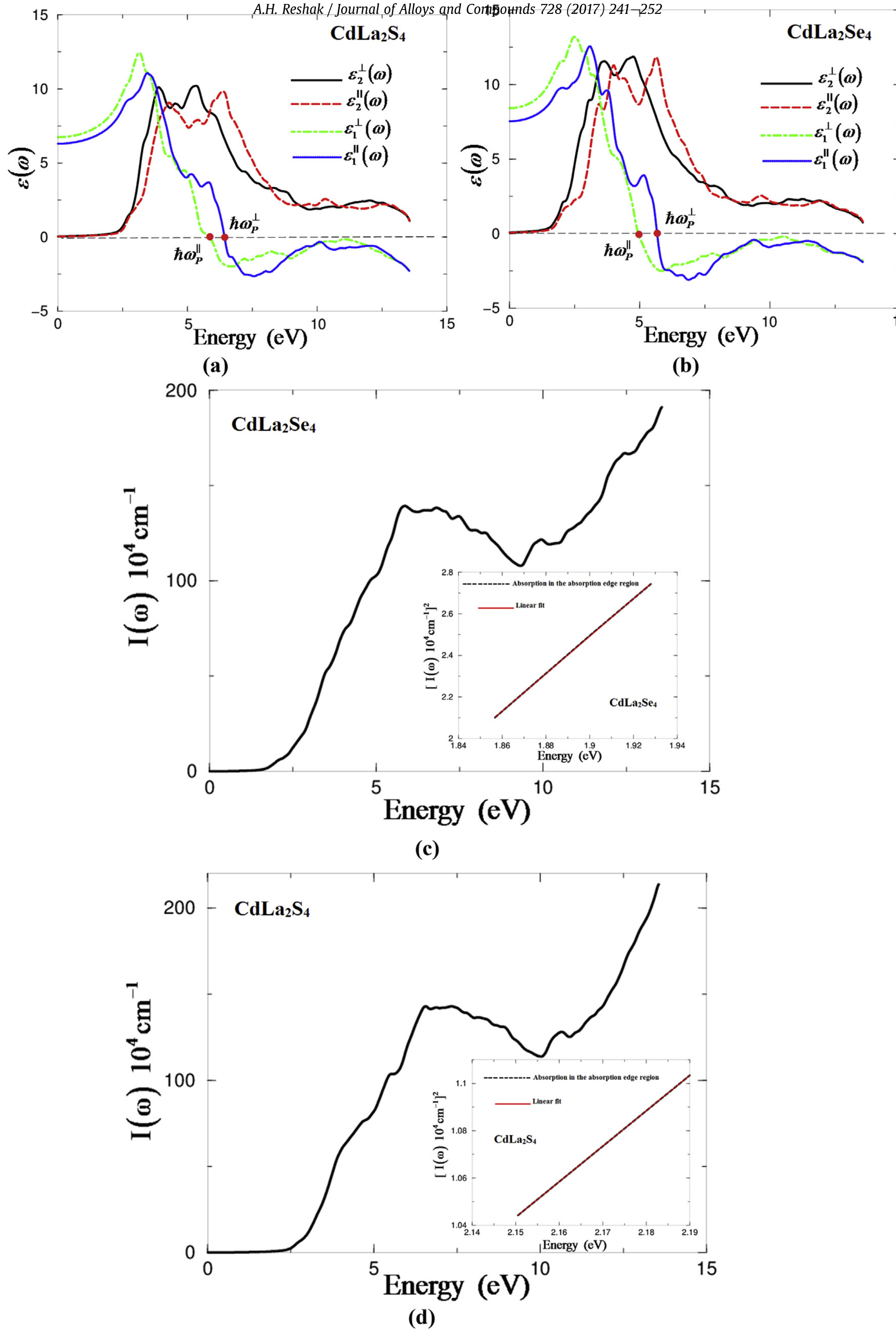

Fig. 2. (a) Calculated $\varepsilon_2^{\perp}(\omega)$ (dark solid curve-black color online), $\varepsilon_2^{\parallel}(\omega)$ (light long dashed curve-red color online) along with Calculated $\varepsilon_1^{\perp}(\omega)$ (dashed doted curve-green color online), $\varepsilon_1^{\parallel}(\omega)$ (doted curve-blue color online) for $CdLa_2S_4$; **(b)** Calculated $\varepsilon_2^{\perp}(\omega)$ (dark solid curve-black color online), $\varepsilon_2^{\parallel}(\omega)$ (light long dashed curve-red color online) along with Calculated $\varepsilon_1^{\perp}(\omega)$ (dashed doted curve-green color online), $\varepsilon_1^{\parallel}(\omega)$ (doted curve-blue color online) for $CdLa_2Se_4$; **(c, d)** Calculated absorption coefficient of $CdLa_2S_4$ and $CdLa_2Se_4$ it is clear that the direct band gap semiconductors have large absorption coefficient (10^4 -10^5 cm^{-1}). The optical band gap's value of the semiconductor materials could be solved as follow; the square of absorption coefficient I(ω) is linear with energy (*E*) for direct optical transitions in the absorption edge region, whereas the square root of I(ω) is linear with *E* for indirect optical transitions. Since the calculated electronic band structure of $CdLa_2S_4$ and $CdLa_2Se_4$ confirms the direct nature of the band gap therefore, the data plots of the square I(ω) versus *E*. It is clearly show that the square I(ω) versus *E* is linear in the absorption edge region. These plots suggest that the absorption edge of $CdLa_2S_4$ and $CdLa_2Se_4$ is caused by direct transitions. We can conclude that the absorption edges of $CdLa_2S_4$ and $CdLa_2Se_4$ occurs at $\lambda = 579.3$ nm, and $\lambda = 670.1$ nm, and the optical band gaps are estimated

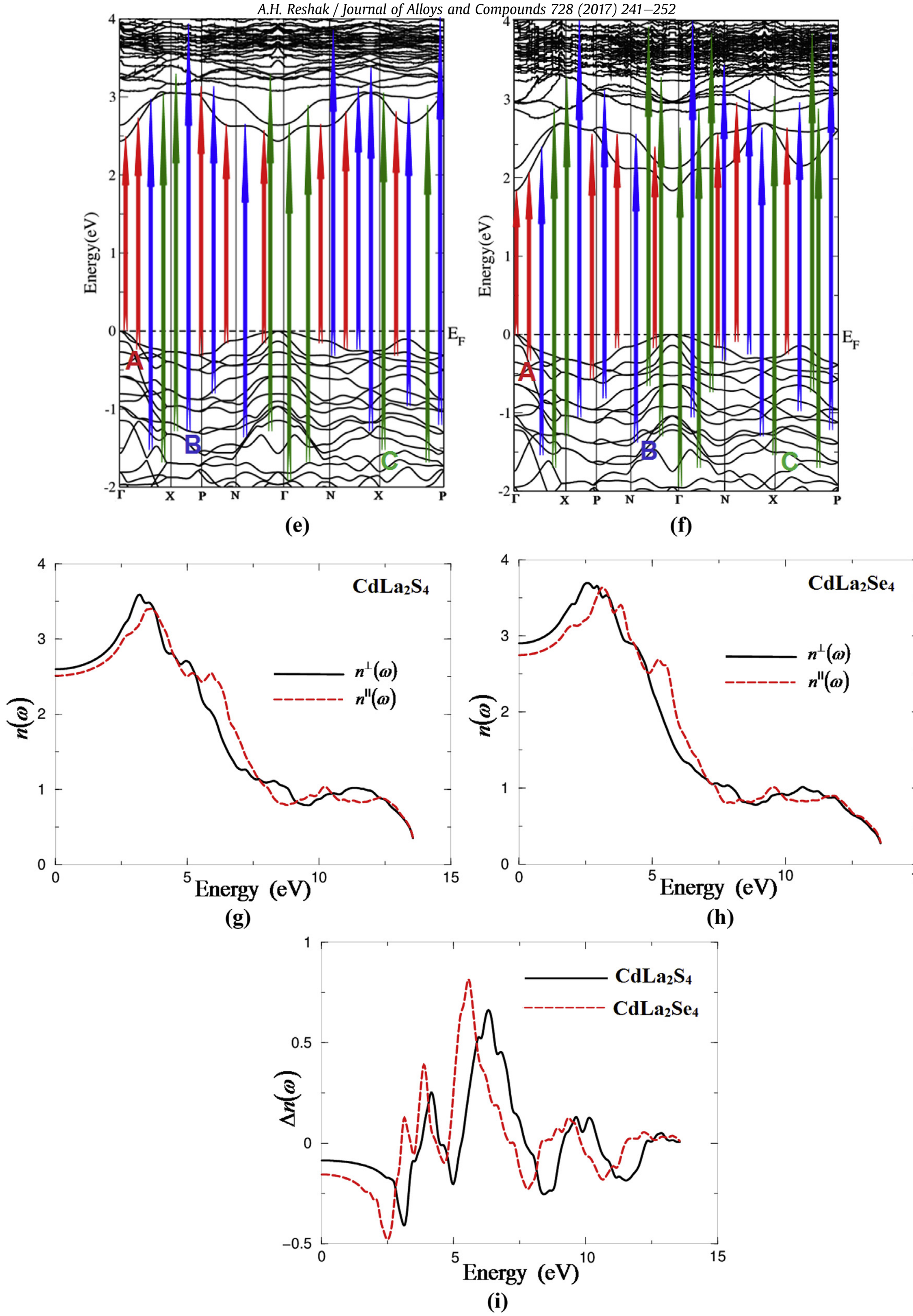

Fig. 2. (*continued*).

to be 2.14 eV, and 1.85 eV for $CdLa_2S_4$ and $CdLa_2Se_4$, respectively; **(e, f)** The optical transitions depicted on a generic band structure of $CdLa_2S_4$ and $CdLa_2Se_4$; **(h, g)** Calculated $n^{\perp}(\omega)$ (dark solid curve-black color online), $n^{\parallel}(\omega)$ (light long dashed curve-red color online) for $CdLa_2S_4$ and $CdLa_2Se_4$; **(i)** Calculated $\Delta n(\omega)$ (dark solid curve-black color online) for $CdLa_2S_4$ and (light long dashed curve-red color online) for $CdLa_2Se_4$; **(j, k)** Calculated $R^{\perp}(\omega)$ (dark solid curve-black color online), $R^{\parallel}(\omega)$ (light long dashed curve-red color online) for $CdLa_2S_4$ and $CdLa_2Se_4$; **(l, m)** Calculated $\sigma_2^{\perp}(\omega)$ (dark solid curve-black color online), $\sigma_2^{\parallel}(\omega)$ (light long dashed curve-red color online) along with Calculated $\sigma_1^{\perp}(\omega)$ (dashed doted curve-green color online), $\sigma_1^{\parallel}(\omega)$ (doted curve-blue color online) for $CdLa_2S_4$ and $CdLa_2Se_4$; **(n,o)** Calculated $L^{\perp}(\omega)$ (dark solid curve-black color online), $L^{\parallel}(\omega)$ (light long dashed curve-red color online) for $CdLa_2S_4$ and $CdLa_2Se_4$. (For interpretation of the references to colour in this figure legend, the reader is referred to the web version of this article.)

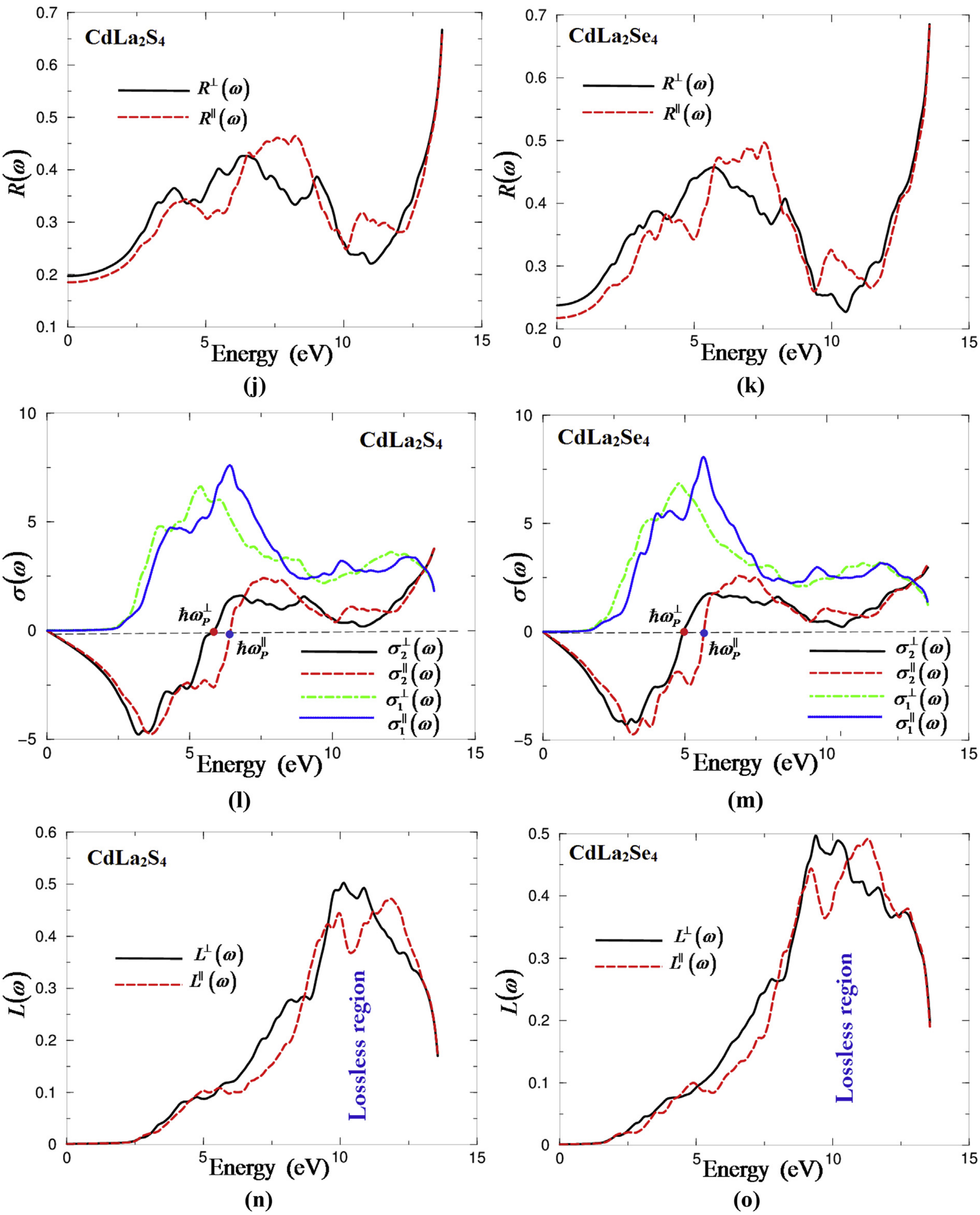

Fig. 2. (*continued*).

$$\chi^{ijk}_{\text{mod}}(-2\omega;\omega,\omega)=\frac{e^3}{2\hbar^2}\int\frac{d\vec{k}}{4\pi^3}\left[\sum_{nml}\frac{f_{nm}}{\omega^2_{mn}(\omega_{mn}-\omega)}\left\{\omega_{nl}\vec{r}^{\,i}_{lm}\left\{\vec{r}^{\,j}_{mn}\vec{r}^{\,k}_{nl}\right\}-\omega_{lm}\vec{r}^{\,i}_{nl}\left\{\vec{r}^{\,j}_{lm}\vec{r}^{\,k}_{mn}\right\}\right\}-i\sum_{nm}\frac{f_{nm}\vec{r}^{\,i}_{nm}\left\{\vec{r}^{\,j}_{mn}\Delta^k_{mn}\right\}}{\omega^2_{mn}(\omega_{mn}-\omega)}\right] \tag{4}$$

From these formulae we can notice that there are three major contributions to $\chi^{(2)}_{ijk}(-2\omega;\omega;\omega)$: the inter-band transitions $\chi^{ijk}_{\text{inter}}(-2\omega;\omega,\omega)$, the intra-band transitions $\chi^{ijk}_{\text{intra}}(-2\omega;\omega,\omega)$ and the modulation of inter-band terms by intra-band terms $\chi^{ijk}_{\text{mod}}(-2\omega;\omega,\omega)$, where $n\neq m\neq l$. Here n denotes the valence states, m the conduction states and l denotes all states($l\neq m,n$). There are two kinds of transitions that can take place, one of them vcc', involves one valence band (v) and two conduction bands ($c$and c'), and the second transition $vv'c$, involves two valence bands (v and v') and one conduction band (c). The symbols are defined as $\Delta^i_{nm}(\vec{k})=\vartheta^i_{nn}(\vec{k})-\vartheta^i_{mm}(\vec{k})$ with $\vec{\vartheta}^{\,i}_{nm}$ being the i component of the electron velocity given as $\vartheta^i_{nm}(\vec{k})=i\omega_{nm}(\vec{k})r^i_{nm}(\vec{k})$ and $\{r^i_{nm}(\vec{k})r^j_{ml}(\vec{k})\}=\frac{1}{2}(r^i_{nm}(\vec{k})r^j_{ml}(\vec{k})+r^j_{nm}(\vec{k})r^i_{ml}(\vec{k}))$. The position matrix elements between band states n and m, $r^i_{nm}(\vec{k})$, are calculated from the momentum matrix element P^i_{nm} using the relation [44]: $r^i_{nm}(\vec{k})=\frac{P^i_{nm}(\vec{k})}{im\omega_{nm}(\vec{k})}$, with the energy difference between the states n and m given by $\hbar\omega_{nm}=\hbar(\omega_n-\omega_m)$. $f_{nm}=f_n-f_m$ is the difference of the Fermi distribution functions. i, j and k correspond to cartesian indices. It has been demonstrated by Aspnes [50] that only the one-electron virtual transitions (transitions between one valence band state and two conduction band statesvcc') give a significant contribution to the second-order tensor. We ignore the virtual-hole contribution (transitions between two valence band states and one conduction band state, $vv'c$) because it was found to be negative and more than an order of magnitude smaller than the virtual-electron contribution for the considered compounds. For simplicity, we denote $\chi^{(2)}_{ijk}(-2\omega;\omega;\omega)$ by Refs.$\chi^{(2)}_{ijk}(\omega)$ [46–50]. The subscripts i, j, and k are cartesian indices.

3. Results and discussion

3.1. Complex first-order linear optical dispersion

Analyzing the electronic distribution is an important factor to investigate the origin of optical properties [45,51]. Deep insight into the electronic structure can be obtained from analyzing the electron cloud of the CdX_4 and LaX_4 units (Fig. 1 c–g). The electron cloud of the CdX_4 groups exhibits a planar shape with conjugated electron orbitals (Fig. 1(e)) shows a high electron density configuration and a strong anisotropy for Cd-X bonds, resulting in the optical anisotropy of CdX_4 groups. The charge localizes mainly between Cd and the neighboring S or Se atoms in CdX_4 unit, also between La and S or Se atoms in LaX_4 unit indicating a partial ionic and strong covalent bonding. The strength of the interactions between the atoms is due to the degree of the hybridization and the electronegativity differences. Also, due to the electronegativity differences between the atoms, some valence electrons are transferred to S or Se atoms and these atoms are surrounded by uniform blue spheres which indicate the maximum charge accumulation according to thermoscale (Fig. 1(d)). The Cd–S, Cd–Se, La–S and La–Se units possess strong electron cloud overlap and prefer to attract holes and repel electrons this in turn enhances the optical activity. The figures bring a clear visualization helpful to understand the origin of the optical properties of these two compounds. The covalent bonding is more favorable for the carrier transport than the ionic one [52]. This may be one of the reasons for the strong linear and nonlinear optical properties in $CdLa_2S_4$ and $CdLa_2Se_4$. The electron cloud of the CdX_4 groups exhibits a planar shape with conjugated electron orbitals. Thus, CdX_4 can be the source of the large birefringence in $CdLa_2S_4$ and $CdLa_2Se_4$. It is well-known that the birefringence determines partly whether an NLO material has the value of study [53–56]. Furthermore, Fig. 1(c–g) show a high electron density configuration and strong anisotropy for Cd-X groups, which indicates the main contribution of CdX_4 groups to the optical anisotropy.

The optical properties can provide more detailed information about the electronic structure of the materials. It is well-known that the optical properties are very sensitive to the energy band gap. In the density functional theory (DFT), by solving the Kohn-Sham equations, we map an interacting many-body system to a non-interacting hypothetical system which has the same electron density. The price that we will pay is the definition of a new functional that is called the exchange-correlation functional. Unfortunately, the exact form of exchange-correlation functional is unknown. Therefore, the accuracy of our results will be sensitive to selection of the exchange-correlation functional and it can play a major role in the accuracy of our results, and this is one of the main questions in DFT. Thus, based on our previous experiences with using mBJ, we have used mBJ to calculate the electronic band structures and hence the optical properties of $CdLa_2S_4$ and $CdLa_2Se_4$ [57,58]. The imaginary part of the linear optical properties $\varepsilon^{xx}_2(\omega)$, $\varepsilon^{yy}_2(\omega)$and $\varepsilon^{zz}_2(\omega)$ for the tetragonal system ($CdLa_2S_4$ and $CdLa_2Se_4$) are calculated and presented in Fig. 2(a and b). It has been noticed that the substitution of S by Se leads to a shift of the whole spectral structure towards lower energies and increase the magnitudes of the optical components.

The spectral structure of $CdLa_2S_4$ and $CdLa_2Se_4$ exhibits two main peaks for $\varepsilon^{\perp}_2(\omega)$ and $\varepsilon^{\parallel}_2(\omega)$ components with small humps situated on the left and right shoulders. The absorption edges occur at 2.14 eV ($CdLa_2S_4$) and 1.85 eV ($CdLa_2Se_4$), as shown in Fig. 2(a and b) and it is confirmed by the calculated absorption coefficients shown in Fig. 2(c and d), which show these compounds possess large absorption coefficient (10^4 cm^{-1}). The optical band gap is crucial for elucidation of the linear and nonlinear optical properties since the energy band gap value appears in the denominator of the equations used to calculate the linear and nonlinear optical properties [eqs. (1)–(4)]. The optical band gap value of the semiconductor materials could be solved as follow; the square of absorption coefficient $\text{I}(\omega)$ is linear with energy (E) for direct optical transitions in the absorption edge region, whereas the square root of I(ω) is linear with E for indirect optical transitions [59,60]. Since the calculated electronic band structure of $CdLa_2S_4$ and $CdLa_2Se_4$ confirms the direct nature of the band gap, the data plots of the square I(ω) versus E are shown in Fig. 2 (c, d). It is clearly show that the square I(ω) versus E is linear in the absorption edge region. These plots suggest that the absorption edges of $CdLa_2S_4$ and $CdLa_2Se_4$ are caused by direct transitions. Following Fig. Fig. 2 (c, d), we can conclude that the absorption edges of $CdLa_2S_4$ and $CdLa_2Se_4$ occur at $\lambda = 579.3$ nm, and $\lambda = 670.1$ nm. The optical band gaps are estimated ($\lambda_g = 1239.8/E_{g(optical)}$ [61]) to be 2.14 eV, and 1.85 eV for $CdLa_2S_4$ and $CdLa_2Se_4$, respectively. The obtained band gap of $CdLa_2S_4$ show good agreement with the available experimental data (2.39 eV) [18,62] and much better than the reported values 1.785 eV ($CdLa_2S_4$) and 1.099 eV ($CdLa_2Se_4$) using VASP code within GGA [28,29], due to the fact that GGA use to underestimated the energy band gap value [63]. The mBJ is a modified Becke-Johnson potential, which allows the calculation of the energy band gap with accuracy similar to that of the very expensive GW calculations [27]. It is a local approximation to an atomic “exact-exchange” potential and a screening term.

The absorption edges of $CdLa_2S_4$ ($CdLa_2Se_4$) are originated from the optical transitions between S-p, La-d (Se-p, La-d) and Cd-s, S-p, La-d (Cd-s, Se-p, La-d) states. It is clear that the Cd orbitals exhibit an insignificant contribution to CBM and VBM; thus, variations in divalent elements can be systematically explored to assess the effects on SHG efficiencies, as well as other attractive properties, while maintaining a wide band gap [64]. The optical transitions are calculated from the momentum matrix elements between the occupied and unoccupied bands, giving rise to the selection rules, as shown in Fig. 2(e and f). In order to identify the observed spectral structures we need to look at the magnitude of the optical matrix elements. The observed spectral structures would correspond to those transitions that have large optical matrix elements. We have used our calculated electronic band structure to map the allowed optical transitions following the selection rules. For simplicity, we have labeled the optical transitions as A, B, and C. The A transitions are responsible for the optical spectral structures between (0.0–5.0) eV, the B transitions represent (5.0–10.0) eV and the C transitions represent the spectral structures between (10.0–14.0) eV (see Fig. 2(e and f)).

Furthermore, the calculated real part of the optical dielectric function can give information about the energy gap since the calculated static electronic dielectric constant by $\varepsilon_\infty = \varepsilon_1(0)$ is inversely related to the energy gap, this could be explained on the basis of the Penn model [65]. As it is clear that the values of $\varepsilon_1^{\perp}(0)$ and $\varepsilon_1^{\parallel}(0)$ for $CdLa_2S_4$ are lower than those obtained for $CdLa_2Se_4$, hence higher $\varepsilon_1(0)$ exhibits a lower energy gap. This supports our finding that substituting S by Se cause a band gap reduction. The calculated values of $\varepsilon_1^{\perp}(0)$ and $\varepsilon_1^{\parallel}(0)$ along with the calculated plasmon oscillations $\omega_p^{\perp}$ and $\omega_p^{\parallel}$ for both compounds are presented in Table 1. The plasmon oscillations are associated with inter-band transitions that occur at energy where optical spectra of the real part crosses zero. The optical components exhibit a considerable anisotropy; this is one of the important features of the optical spectra. The other important feature is the uniaxial anisotropy ($\delta\varepsilon$) which can be obtained from $\varepsilon_1^{\perp}(0)$ and $\varepsilon_1^{\parallel}(0)$. Following Fig. 2(a and b), we found that both compounds possess negative $\delta\varepsilon$, as shown in Table 1.

The calculated refractive indices $n^{\perp}(\omega)$ and $n^{\parallel}(\omega)$ of $CdLa_2S_4$ and $CdLa_2Se_4$ as derived from the complex dielectric functions are presented in Fig. 2(g and h). Thus, the birefringence can be estimated from $\Delta n(\omega) = n_e(\omega) - n_o(\omega)$. It was found that both compounds exhibit negative birefringence at the static limit, as shown in Table 1. We found that the $\Delta n(0)$ for $CdLa_2S_4 > CdLa_2Se_4$; hence $CdLa_2Se_4$ exhibits weaker anisotropy. The birefringence is necessary to fulfill the phase-matching condition. Therefore, we expected $CdLa_2Se_4$ will produce higher second harmonic generation than $CdLa_2S_4$. The dispersion of the birefringence of the two compounds is illustrated in Fig. 2(i).

The optical reflectivity spectra of $CdLa_2S_4$ and $CdLa_2Se_4$ along the [100], [101] and [001] polarization directions are shown in Fig. 2(j and k). It was been found that at low energies the compounds exhibit low reflectivity. The first reflectivity maxima occur at around 7.0 eV, followed by the first reflectivity minima which is situated at around 11.0 eV, confirming the occurrence of a collective plasmon resonance in concordance with our observation in Fig. 2(a and b). At higher energies the region confined between 12.0 and 12.0 eV represents the lossless region.

The optical conductivity (Fig. 2 l,m) can be obtained from the complex first-order linear optical dielectric function following the expression $\varepsilon(\omega) = \varepsilon_1(\omega) + i\varepsilon_2(\omega) = 1 + \frac{4\pi i\sigma(\omega)}{\omega}$. It consists of imaginary and real parts; therefore, it completely characterizes the linear optical properties. The imaginary part $\sigma_2^{\perp}(\omega)$ and $\sigma_2^{\parallel}(\omega)$ between 0.0 and the values of $\omega_p^{\perp}$ and $\omega_p^{\parallel}$ exhibit overturned features of $\varepsilon_2^{\perp}(\omega)$ and $\varepsilon_2^{\parallel}(\omega)$, whereas the real parts $\sigma_1^{\perp}(\omega)$ and $\sigma_1^{\parallel}(\omega)$ show similar features to those of $\varepsilon_2^{\perp}(\omega)$ and $\varepsilon_2^{\parallel}(\omega)$. The intersection of the imaginary and real parts of the optical conductivity at the zero energy represents the values of $\omega_p^{\perp}$ and $\omega_p^{\parallel}$. The loss function peaks (Fig. 2 n,o), are initiated at the values of the plasma frequencies $\omega_p^{\perp}$ and $\omega_p^{\parallel}$ at the energy point where optical spectra of $\varepsilon_1^{\perp}(\omega)$ and $\varepsilon_1^{\parallel}(\omega)$ cross zero.

3.2. Complex second-order non-linear optical dispersion

Since the nonlinear optical properties are very sensitive to the energy band gap values due to the fact that the band gap value comes in the denominator of the complex nonlinear optical formulas [eqs. (2)–(4)] which are used to calculate the complex nonlinear optical susceptibility. Therefore, to achieve appropriate results, an accurate energy band gap is required, and, to achieve this, the mBJ approximation was applied. Furthermore, a quasi-particle self-energy correction at the level of scissors operators is applied to avoid the DFT drawback. In the scissors operators, the energy bands are rigidly shifted to merely bring the DFT band gap to the exact experimental value. The tetragonal symmetry (I-42d) allows only two non-zero tensor components. These are

Table 1
The calculated energy band gap in comparison with the experimental value, $\varepsilon_1^{\perp}(0), \varepsilon_1^{\parallel}(0), \delta\varepsilon, \omega_p^{\perp}, \omega_p^{\parallel}, n^{\perp}(0), n^{\parallel}(0)$and $\Delta n(0)$.

	$CdLa_2S_4$		$CdLa_2Se_4$	
	This work	other	This work	other
Eg (eV)	2.14	2.39[a], 1.785[b]	1.85	1.099[c]
$\varepsilon_1^{\perp}(0)$	6.749		8.424	
$\varepsilon_1^{\parallel}(0)$	6.311		7.546	
$\delta\varepsilon$	−0.070		−0.109	
$\omega_p^{\perp}$	5.864		4.966	
$\omega_p^{\parallel}$	6.435		5.673	
$n^{\perp}(0)$	2.598		2.902	
$n^{\parallel}(0)$	2.512		2.747	
$\Delta n(0)$	−0.086		−0.155	

[a] Refs. [18, 62].
[b] Ref. [28].
[c] Ref. [29].

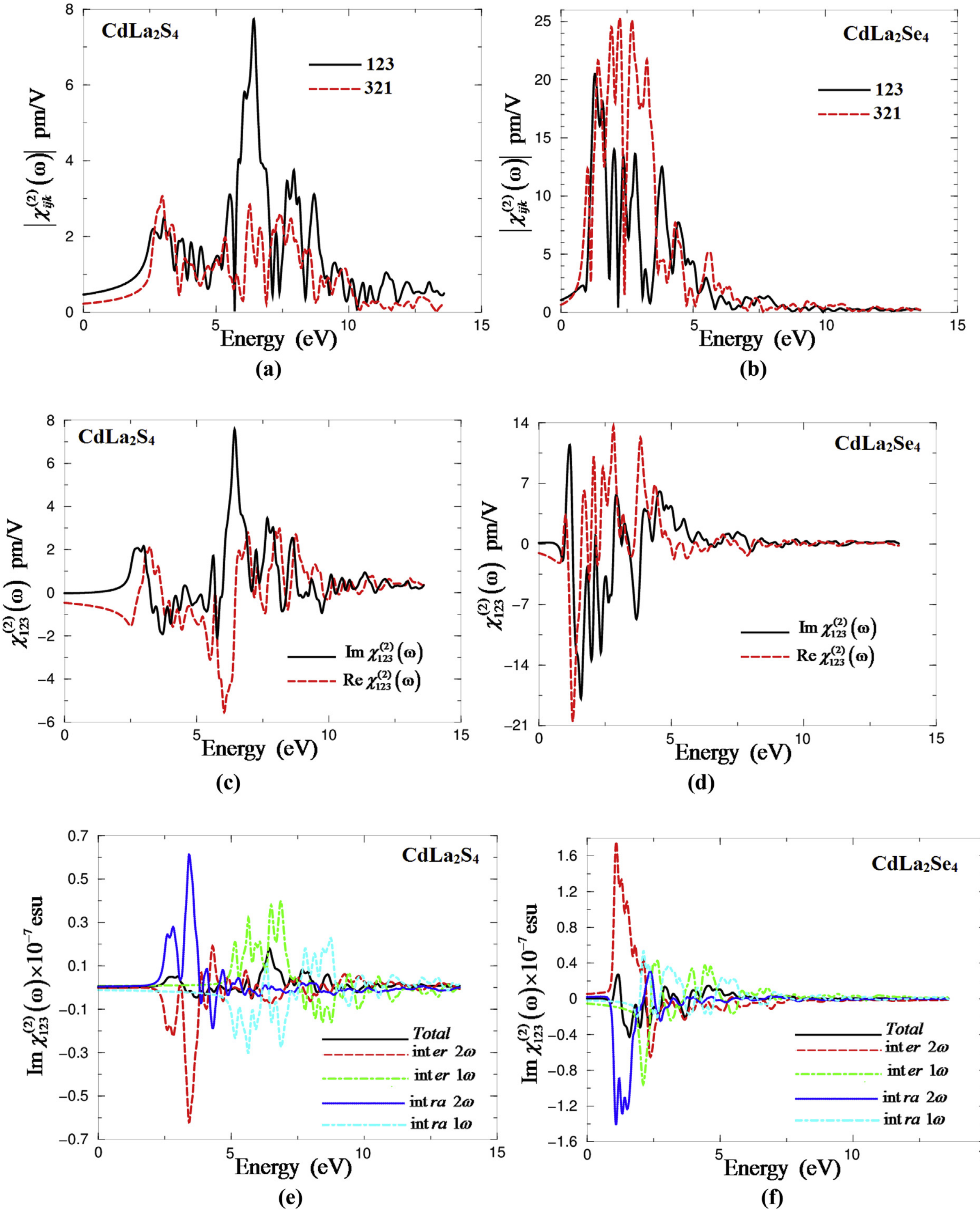

Fig. 3. **(a)** Calculated $\left|\chi^{(2)}_{ijk}(\omega)\right|$ for the two tensor components of $CdLa_2S_4$; **(b)** Calculated $\left|\chi^{(2)}_{ijk}(\omega)\right|$ for the two tensor components of $CdLa_2Se_4$; **(c)** Calculated Imaginary $\chi^{(2)}_{123}(\omega)$(**dark solid curve-black color online**) and real $\chi^{(2)}_{123}(\omega)$ (light dashed curve-red color online) spectra of $CdLa_2S_4$; **(d)** Calculated Imaginary $\chi^{(2)}_{123}(\omega)$(**dark solid curve-black color online**) and real $\chi^{(2)}_{123}(\omega)$ (light dashed curve-red color online) spectra of $CdLa_2Se_4$; (**e, f**) Calculated total Im$\chi^{(2)}_{123}(\omega)$ spectrum (**dark solid curve-black color online**) along with the intra (2ω)/(1ω) (light solid curve-blue color online)/(light dashed doted curve-cyan color online) and inter (2ω)/(1ω) (light long dashed curve-red color online)/(light doted curve-green color online) -band contributions of $CdLa_2S_4$ and $CdLa_2Se_4$, here all Im$\chi^{(2)}_{123}(\omega)$ are multiplied by 10^{-7}, in esu units; (**g,h**) –***upper panel***- Calculated $\left|\chi^{(2)}_{123}(\omega)\right|$(dark solid curve-black color online); -*lower panel*- Calculated $\varepsilon_2(\omega)$ (**dark solid curve-black color online**); Calculated $\varepsilon_2(\omega/2)$ (**dark dashed curve-red color online**) of $CdLa_2S_4$ and $CdLa_2Se_4$. (For interpretation of the references to colour in this figure legend, the reader is referred to the web version of this article.)

$\chi^{(2)}_{123}(-2\omega;\omega;\omega)$ and $\chi^{(2)}_{321}(-2\omega;\omega;\omega)$. Fig. 3 (a, b) show the calculated absolute values $\left|\chi^{(2)}_{ijk}(-2\omega;\omega;\omega)\right|$of those two tensor components for $CdLa_2S_4$ and $CdLa_2Se_4$. These figures reveals that the $\left|\chi^{(2)}_{123}(-2\omega;\omega;\omega)\right|$ is the dominant one, since it shows higher

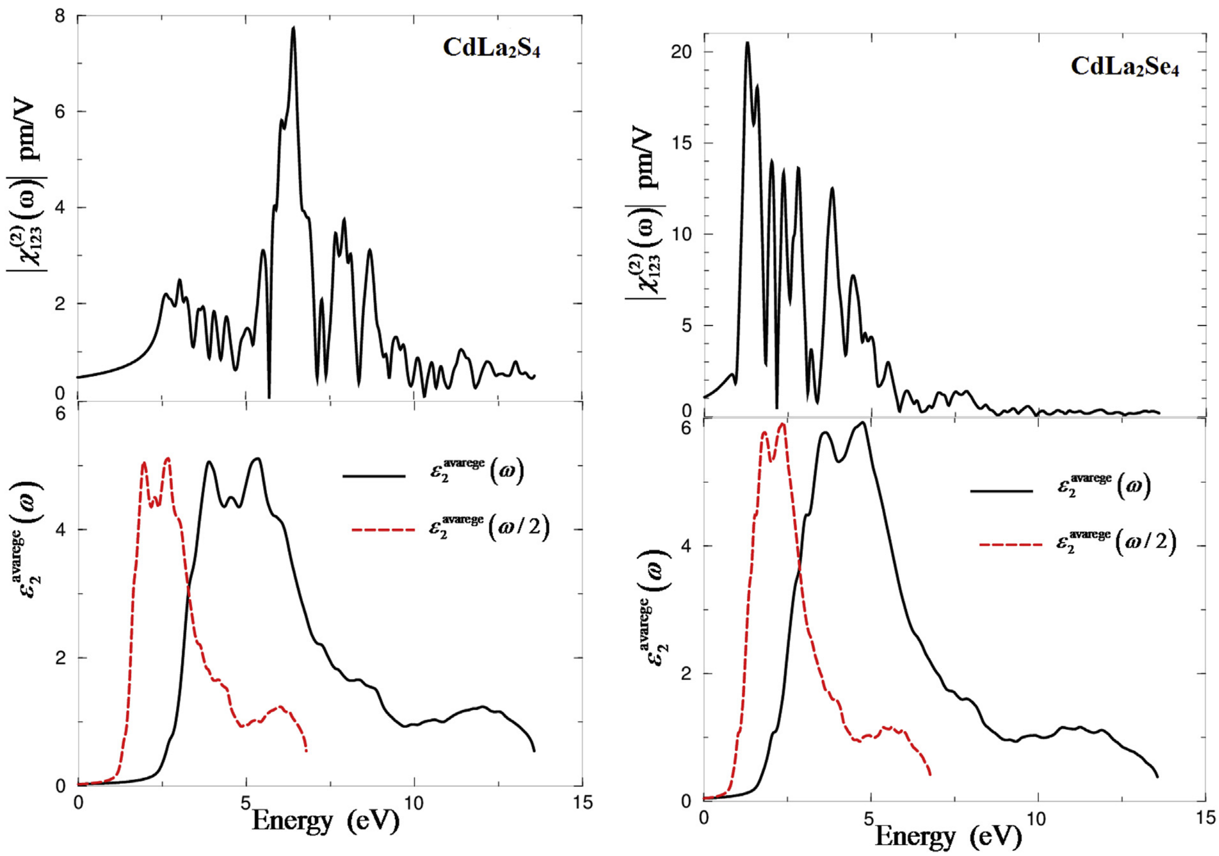

(g) (h)

Fig. 3. (*continued*).

value than that of $\left|\chi^{(2)}_{321}(-2\omega;\omega;\omega)\right|$, as shown in Tables 2 and 3. Following these results, one can see that $CdLa_2S_4$ exhibits SHG intensity of about two times of the well-known KH_2PO_4 (KDP) crystal which exhibits a SHG value of 0.39 p.m./V at $\lambda = 1064$ nm [66]. Whereas, $CdLa_2Se_4$ exhibits SHG very close to the experimental value of the well-known $KTiOPO_4$ (KTP) single crystals which possesses a SHG value of about 16.9 [67], 13.7 [68], 15.4 ± 0.2 [69],

Table 2
Calculated $\left|\chi^{(2)}_{ijk}(\omega)\right|$ and β_{ijk} of $\mathbf{CdLa_2S_4}$, in pm/V at static limit and at $\lambda = 1064$ nm, in comparison with the experimental value of the well known KH_2PO_4 (KDP) single crystals which exhibits a SHG value of about 0.39 p.m./V at $\lambda = 1064$ nm [66]. Where 1 p.m./V = 2.387×10^{-9} esu.

$CdLa_2S_4$				
Tensor components	$\chi^{(2)}_{ijk}(0)$	Theory $d_{ijk} = 0.5\chi^{(2)}_{ijk}(\omega)$	$\chi^{(2)}_{ijk}(\omega)$ at $\lambda = 1064$	Theory $d_{ijk} = 0.5\chi^{(2)}_{ijk}(\omega)$
$\left|\chi^{(2)}_{123}(\omega)\right|$	0.451	$d_{14=}$0.225	0.639	$d_{14=}$0.319
$\left|\chi^{(2)}_{321}(\omega)\right|$	0.216	$d_{36=}$0.108	0.319	$d_{36=}$0.159
β_{333}	0.326×10^{-30} esu		0.453×10^{-30} esu	

Table 3
Calculated $\left|\chi^{(2)}_{ijk}(\omega)\right|$ and β_{ijk} of $\mathbf{CdLa_2Se_4}$ in pm/V at static limit and at $\lambda = 1064$ nm, in comparison with the experimental value of the well known $KTiOPO_4$ (KTP) single crystals which exhibits a SHG value of about 16.9 [67], 13.7 [68], 15.4 ± 0.2 [69], 14.6 ± 1.0 [70], 17.4 ± 1.7 [71], 16.9 ± 3.3 [72], 16.9 ± 1.7 [73], 10.6 ± 7.5 [74], 16.75 [75] and 16.65 [75] at $\lambda = 1064$ nm. Where 1 p.m./V = 2.387×10^{-9} esu.

$CdLa_2Se_4$				
Tensor components	$\chi^{(2)}_{ijk}(0)$	Theory $d_{ijk} = 0.5\chi^{(2)}_{ijk}(\omega)$	$\chi^{(2)}_{ijk}(\omega)$ at $\lambda = 1064$	Theory $d_{ijk} = 0.5\chi^{(2)}_{ijk}(\omega)$
$\left|\chi^{(2)}_{123}(\omega)\right|$	1.087	$d_{14=}$0.543	14.871	$d_{14=}$7.435
$\left|\chi^{(2)}_{321}(\omega)\right|$	0.678	$d_{36=}$0.339	7.011	$d_{36=}$3.505
β_{333}	0.922×10^{-30} esu		12.090×10^{-30} esu	

14.6 ± 1.0 [70], 17.4 ± 1.7 [71], 16.9 ± 3.3 [72], 16.9 ± 1.7 [73], 10.6 ± 7.5 [74], 16.75 [75] and 16.65 [75] at $\lambda = 1064$ nm. It is clear that $CdLa_2Se_4$ exhibits larger nonlinear optical properties than that of $CdLa_2S_4$, and the cost of good SHG performance is the narrower band gap, which limits the transmittance range. The main point to obtain NLO materials is getting the delicate balance between the SHG response and band gap [76].

The real and imaginary parts of $\chi^{(2)}_{123}(-2\omega;\omega;\omega)$ for $CdLa_2S_4$ and $CdLa_2Se_4$ are presented in Fig. 3 (c, d). These figures show that the Im $\chi^{(2)}_{123}(-2\omega;\omega;\omega)$ value rises at a half value of the energy band gap due to 2ω terms oscillation, then at the exact value of the fundamental gap the ω terms start to oscillate to be added to 2ω terms. While at higher energies only ω terms will contribute. To analyze the spectral features of the Im$\chi^{(2)}_{123}(-2\omega;\omega;\omega)$, we have calculated the $2\omega/\omega$ inter-/intra-band contributions to explore the origin of the strong SHG in these compounds, as shown in Fig. 3(e and f). For deep investigation, the spectral structure of the dominant component is drawn in associated with the absorptive part of the corresponding dielectric function $\varepsilon_2(\omega)$ as a function of $\omega/2$and ω , to identify the origin of the spectral peaks as caused by $2\omega/\omega$ inter-/intra-band contributions. These are shown in Fig. 3(g and h), the first structure in $\left|\chi^{(2)}_{123}(\omega)\right|$ between 1.19 and 2.39 eV (0.93–1.85 eV) for $CdLa_2S_4$ ($CdLa_2Se_4$) is mainly originated from 2ω resonance [see $\varepsilon_2(\omega/2)$ Fig. 3(g and h) -lower panel]. The second structure between 2.39 and 5.0 eV (1.85–5.0 eV) is associated with interference between 2ω andω resonances (the threshold of $\varepsilon_2(\omega)$) [see $\varepsilon_2(\omega/2)$and $\varepsilon_2(\omega)$ Fig. 3(g and h) –lower panel]. The last spectral structure from 5.0 and above is mainly due to ω resonance and it is associated with the second structure in $\varepsilon_2(\omega)$. With the aid of the existing values of the SHG for the dominant components of $CdLa_2S_4$ and $CdLa_2Se_4$, we obtained the values of the microscopic first hyperpolarizability, β_{123} [77,78], the vector component along the dipole moment direction, at the static limit and at $\lambda = 1064$ nm. These values are listed in Tables 2 and 3 In general, the microscopic first hyperpolarizability term, β_{ijk}, cumulatively yield a bulk observable second order susceptibility term, $\chi^{(2)}_{ijk}(\omega)$, which in turn is responsible for the high SHG response [77,78].

4. Conclusions

The influence of replacing S by Se on the linear and nonlinear optical susceptibilities in $CdLa_2S_4$ and $CdLa_2Se_4$ was investigated by means of DFT. The all-electron full-potential linearized augmented plane wave plus local orbitals (FP-LAPW + lo) method was used. Using PBE-GGA, the experimental geometries of $CdLa_2S_4$ and $CdLa_2Se_4$ were optimized by minimizing the forces acting on the atoms. The resulting geometries were used to calculate the linear and nonlinear optical susceptibilities using mBJ potential. It was been found that mBJ succeeds by a large amount in bringing the calculated energy gap closer to the experimental one. The calculation shows the direct band nature of the investigated compounds. The valence electronic charge density exhibits a clear visualization to understand the origin of linear and nonlinear optical susceptibilities. The linear optical properties exhibit considerable anisotropy that is favorable to enhance the spectral range for frequency conversion. $CdLa_2S_4$ exhibits SHG of about two times of the well-known KH_2PO_4 (KDP) single crystals which exhibits a SHG value of 0.39 p.m./V. Whereas $CdLa_2Se_4$ exhibits SHG very close to the experimental value of the well-known $KTiOPO_4$ (KTP) single crystals which exhibits a SHG value of about 16.9, 13.7, 15.4 ± 0.2, 14.6 ± 1.0, 17.4 ± 1.7, 16.9 ± 3.3, 16.9 ± 1.7, 10.6 ± 7.5, 16.75 and 16.65.

Author contribution

A. H. Reshak, as a professor with PhD in physics and PhD in materials engineering has performed the calculations, analyzing and discussing the results and writing the manuscript.

Competing financial interests

The author declare no competing financial interests.

Acknowledgments

The result was developed within the CENTEM project, reg. no. CZ.1.05/2.1.00/03.0088, cofunded by the ERDF as part of the Ministry of Education, Youth and Sports OP RDI programme and, in the follow-up sustainability stage, supported through CENTEM PLUS (LO1402) by financial means from the Ministry of Education, Youth and Sports under the "National Sustainability Programme I. Computational resources were provided by MetaCentrum (LM2010005) and CERIT-SC (CZ.1.05/3.2.00/08.0144) infrastructures.

References

[1] D. Xue, Z. Zhang, Appl. Phys. A 68 (1999) 57–61.
[2] C.T. Chen, Y.C. Wu, A.D. Jiang, B.C. Wu, G.M. You, R. Li, S. Lin, J. Opt. Soc. Am. B 6 (1989) 616–621.
[3] P.S. Halasyamani, K.R. Poeppelmeier, Chem. Mater. 10 (1998) 2753–2769.
[4] P.A. Maggard, C.L. Stern, K.R. Poeppelmeier, J. Am. Chem. Soc. 123 (2001) 7742–7743.
[5] C.F. Sun, C.L. Hu, X. Xu, B.P. Yang, J.G. Mao, J. Am. Chem. Soc. 133 (2011) 5561–5572.
[6] W.L. Zhang, W.D. Chen, H. Zhang, L. Geng, C.S. Lin, Z.Z. He, J. Am. Chem. Soc. 132 (2010) 1508–1509.
[7] S.L. Pan, J.P. Smit, B. Watkins, M.R. Marvel, C.L. Stern, K.R. Poeppelmeier, J. Am. Chem. Soc. 128 (2006) 11631–11634.
[8] S.J. Choyke, S.M. Blau, A.A. Larner, S.A. Narducci, J. Yeon, P.S. Halasyamani, A. Norquist, J. Inorg. Chem. 48 (2009) 11277–11282.
[9] Zhi-Shu Feng, Zhi-Hui Kang, Feng-Guang Wu, Jin-Yue Gao, Yun Jiang, Hong-Zhi Zhang, Yury M. Andreev, Grigory V. Lanskii, Viktor V. Atuchin, Tatyana A. Gavrilova, Opt. Exp. 16 (13) (2008) 9978–9985.
[10] J.-J. Huang, V.V. Atuchin, Yu. M. Andreev, G.V. Lanskii, N.V. Pervukhina, J. Cryst. Growth 292 (2006) 500–504.
[11] V.V. Atuchin, B.G. Bazarov, T.A. Gavrilova, V.G. Grossman, M.S. Molokeev, Zh.G. Bazarova, J. Alloys Compd. 515 (2012) 119–122.
[12] T. Thao Tran, Nathan Z. Koocher, James M. Rondinelli, P. Shiv Halasyamani, Angew. Chem. Int. Ed. 129 (11) (2017) 3015–3019.
[13] Jiang-He Feng, Chun-Li Hu, Xiang Xu, Bing-Xuan Li, Ming-Jian Zhang, Jiang-Gao Mao, Chem. Eur. J. (2017), http://dx.doi.org/10.1002/chem.201702632.
[14] K.K. Banger, J. Cowen, A.F. Hepp, Chem. Mater. 13 (2001) 3827.
[15] C.M. Joseph, C.S. Menon, Semicond. Sci. Technol. 11 (1996) 1668.
[16] I. Tsuji, H. Kato, A. Kudo, Angew. Chem. Int. Ed. 44 (2005) 3565.
[17] T.N. Meng, B.B. Chris, J. V Jagadese, J. Am. Chem. Soc. 128 (2006) 7118.
[18] Xing Guangjian, Guo Hongli, Li Peng, Wu Guangming, Appl. Mech. Mater. 556–562 (2014) 362–365.
[19] B.B. Kale, J.O. Baeg, K.J. Kong, S.J. Moon, L.K. Nikam, K.R. Patil, J. Mater. Chem. 21 (2011) 2624.
[20] H. Miao, H. Li, Y. Cui, D. Tao, G. Wang, Y. Zhou, Mater. Lett. 133 (2014) 281.
[21] Y.P. Yuan, S.W. Cao, L.S. Yin, L. Xu, C. Xue, Int. J. Hydrogen Energy 38 (2013) 7218.
[22] L. Zhu, W.-C. Oh, RSC Adv. 5 (2015) 90321.
[23] J. Hou, C. Yang, Z. Wang, S. Jiao, H. Zhu, RSC Adv. 2 (2012) 10330.
[24] H. Liu, Z. Xu, Z. Zhang, D. Ao, Appl. Catal. B Environ. 192 (2016) 234.
[25] P. Blaha, K. Schwarz, G.K.H. Madsen, D. Kvasnicka, J. Luitz, WIEN2k, an Augmented Plane Wave Plus Local Orbitals Program for Calculating Crystal Properties, Vienna University of Technology, Austria, 2001.
[26] J.P. Perdew, S. Burke, M. Ernzerhof, Phys. Rev. Lett. 77 (1996) 3865.
[27] F. Tran, P. Blaha, Phys. Rev. Lett. 102 (2009) 226401.
[28] https://materialsproject.org/materials/mp-36395/.
[29] https://materialsproject.org/materials/mp-36733/.
[30] M.I. Kolinko, I.V. Kityk, A.S. Krochuk, J. Phys. Chem. Solid. 53 (1992) 1315–1320.
[31] G.E. Davydyuk, O.Y. Khyzhun, A.H. Reshak, H. Kamarudin, G.L. Myronchuk, S.P. Danylchuk, A.O. Fedorchuk, L.V. Piskach, M. Yu. Mozolyuk, O.V. Parasyuk, Phys. Chem. Chem. Phys. 15 (2013) 6965.
[32] A.H. Reshak, Y.M. Kogut, A.O. Fedorchuk, O.V. Zamuruyeva, G.L. Myronchuk, O.V. Parasyuk, H. Kamarudin, S. Auluck, K.L. Plucinskig, J. Bila, Phys. Chem.

Chem. Phys. 15 (2013) 18979.
[33] V.V. Atuchin, T.A. Gavrilova, J.-C. Grivel, V.G. Kesler, Surf. Sci. 602 (2008) 3095–3099.
[34] V.V. Atuchin, T.A. Gavrilova, J.-C. Grivel, V.G. Kesler, J. Phys. D Appl. Phys. 42 (2009) 035305.
[35] O.Y. Khyzhun, V.L. Bekenev, V.V. Atuchin, E.N. Galashov, V.N. Shlegel, Mater. Chem. Phys. 140 (2013) 558–595.
[36] V.V. Atuchin, E.N. Galashov, O.Y. Khyzhun, V.L. Bekenev, L.D. Pokrovsky, Yu.A. Borovlev, V.N. Zhdankov, J. Solid State Chem. 236 (2016) 24–31.
[37] K. Nouneh, Ali H. Reshak, S. Auluck, I.V. Kityk, R. Viennois, S. Benet, S. Charar, J. Alloy. Comp. 437 (2007) 39–46.
[38] A.H. Reshak, K. Nouneh, I.V. Kityk, Jiri Bila, S. Auluck, H. Kamarudin, Z. Sekkat, Int. J. Electrochem. Sci. 9 (2014) 955–974.
[39] A.H. Reshak, Specific features of electronic structures and optical susceptibilities of molybdenum oxide, RSC Adv. 5 (2015) 22044.
[40] A.H. Reshak, H. Huang, H. Kamarudin, S.J. Auluck, Appl. Phys. 117 (2015) 085703.
[41] A.H. Reshak, RSC Adv. 5 (2015) 33632–33638.
[42] A. H. Reshak, Sci. Rep. | 7:46415 | DOI: 10.1038/srep46415
[43] A.H. Reshak, S. Auluck, RSC Adv. 7 (2017) 14752.
[44] C. Ambrosch-Draxl, J.O. Sofo, Comput. Phys. Comm. 175 (2006) 1–14.
[45] http://www.wien2k.at/reg_user/textbooks/usersguide.pdf.
[46] S. Sharma, C. Ambrosch-Draxl, Phys. Scr. T 109 (2004) 128.
[47] S. Sharma, J.K. Dewhurst, C. Ambrosch-Draxl, Phys. Rev. B 67 (2003) 165332.
[48] S.N. Rashkeev, W.R.L. Lambrecht, B. Segall, Phys. Rev. B 57 (1998) 3905.
[49] J.L.P. Hughes, J.E. Sipe, Phys. Rev. B 53 (1996) 10751.
[50] D.E. Aspnes, Phys. Rev. B 6 (1972) 4648.
[51] Z.S. Lin, J. Lin, Z.Z. Wang, C.T. Chen, M.H. Lee, Phys. Rev. B 62 (2000) 1757–1764.
[52] F. Wu, H.Z. Song, J.F. Jia, X. Hu, Prog. in Nat. Sci.: Mater. Int. 23 (2013) 408–412.
[53] Q. Bian, Z. Yang, L. Dong, S. Pan, H. Zhang, H. Wu, H. Yu, W. Zhao, Qun Jing, J. Phys. Chem. C 118 (44) (2014) 25651–25657.
[54] Yu.M. Andreev, V.V. Atuchin, G.V. Lanskii, N.V. Pervukhina, V.V. Popov, N.C. Trocenco, Solid State Sci. 7 (2005) 1188–1193.
[55] Z.-H. Kang, J. Guo, Z.-S. Feng, J.-Y. Gao, J.-J. Xie, L.-M. Zhang, V. Atuchin, Y. Andreev, G. Lanskii, A. Shaiduko, Appl. Phys. B 108 (2012) 545–552.
[56] V.V. Atuchin, S.V. Adichtchev, B.G. Bazarov, Zh.G. Bazarova, T.A. Gavrilova, V.G. Grossman, V.G. Kesler, G.S. Meng, Z.S. Lin, N.V. Surovtsev, Mater. Res. Bull. 48 (2013) 929–934.
[57] David Koller, Fabien Tran, Peter Blaha, Phys. Rev. B 83 (2011) 195134.
[58] Sergey F. Solodovnikov, Victor V. Atuchin, Zoya A. Solodovnikova, Oleg Y. Khyzhun, Mykola I. Danylenko, Denis P. Pishchur, Pavel E. Plyusnin, Alexey M. Pugachev, Tatiana A. Gavrilova, Alexander P. Yelisseyev, Ali H. Reshak, Zeyad A. Alahmed, Nadir F. Habubi, Inorg. Chem. 56 (2017) 3276–3286.
[59] H. Huang, Y. He, X. Li, M. Li, C. Zeng, F. Dong, X. Du, T. Zhangd, Y. Zhang, J. Mater. Chem. A 3 (2015) 24547–24556.
[60] H. Huang, Y. He, Z. Lin, L. Kang, Y. Zhang, J. Phy. Chem. C 117 (2013) 22986–22994.
[61] J.M. Carlsson, B. Hellsing, H.S. Domingos, P.D. Bristowe, Phys. Rev. B 65 (2002) 205122–205132.
[62] Lei Zhu, Won-Chun Oh, J. Korean Ceram. Soc. 52 (No. 3) (2015) 173–179.
[63] P. Dufek, P. Blaha, K. Schwarz, Phys. Rev. B 50 (1994) 7279.
[64] J.A. Brant, D.J. Clark, Y.S. Kim, J.I. Jang, Zhang Jian-Han, Aitken, J. A. Chem. Mater 26 (2014) 3045–3048.
[65] D.R. Penn, Phys. Rev. B 128 (1962) 2093.
[66] Progress in Photochemistry and Photophysics, Volume 5, 1990 By Jan F. Rabek, ISBN 9780849340451-CAT# 4045.
[67] K. Zhang, X. Wang, Chinese Science Bull. 46 (2001) 2028–2036.
[68] http://www.castech-us.com/casktp.htm.
[69] M.V. Pack, D.J. Armstrong, A.V. Smith, Appl. Optics 43 (2004) 3319.
[70] I. Shoji, T. Kondo, A. Kitamoto, M. Shirane, R. Ito, J. Opt. Soc. Am. B 14 (1997) 2268.
[71] A. Anema, T. Rasing, Appl. Opt 36 (1997) 5902.
[72] L.K. Cheng, L.T. Cheng, J. Galperin, P.A.M. Hotsenpiller, J.D. Bierlein, J. Cryst. Growth 137 (1994) 107–115.
[73] H. Vanherzeele, J.D. Bierlein, Opt. Lett. 17 (1992) 982–984.
[74] B. Boulanger, J.P. Feve, G. Marnier, B. Menaert, Pure Appl. Opt 7 (1998) 239.
[75] A.H. Reshak, I.V. Kityk, S. Auluck, J. Phys. Chem. B 114 (2010) 16705–16712.
[76] D. Li, Q. Jing, C. Lei, S. Pan, B. Zhang, Z. Yang, RSC Adv. 97 (2015) 79882–79887.
[77] R. Boyd, Nonlinear Optics, third ed., Acadmic Press is an imprint of Elsevier, 2008. ISBN:978-0-12-369470-6.
[78] R. Boyd, Principles of Nonlinear Optics, Academic Press, NY, 1982, p. 420.